

Article

Spray-Mediated Air-Sea Gas Exchange: The Governing Time Scales

Edgar L. Andreas¹, Penny Vlahos^{2,*} and Edward C. Monahan²¹ NorthWest Research Associates, Inc., Lebanon, NH 03766-1900 USA; eandreas@nwra.com² Department of Marine Sciences, University of Connecticut, 1080 Shennecossett Road, Groton, CT 06340-6048, USA; edward.monahan@uconn.edu

* Correspondence: penny.vlahos@uconn.edu; Tel.: +1-860-405-9269

Academic Editor: Bronte Tilbrook

Received: 13 November 2017; Accepted: 11 December 2017; Published: 18 December 2017

Abstract: It is not known whether sea spray droplets can act as agents that influence air-sea gas exchange. We begin to address that question here by evaluating the time scales that govern spray-mediated air-sea gas transfer. To move between the interior of a spray droplet and the atmospheric gas reservoir, gas molecules must complete three distinct steps: (1) Gas molecules must mix between the interior surface and the deep interior of the aqueous solution droplet; time scale τ_{aq} estimates the rate of this transfer; (2) Molecules must cross the droplet's interface; time scale τ_{int} parameterizes this transfer; and (3) The molecules must transit a "jump" layer between a spray droplet's exterior surface and the atmospheric gas reservoir; time scale τ_{air} dictates the rate of this transfer. The same steps, in reverse order, pertain to gas molecules moving from an atmospheric reservoir to a drop's interior. For the six most plentiful gases, excluding water vapor, in the atmosphere—helium, neon, argon, oxygen, nitrogen, and carbon dioxide— τ_{air} , τ_{int} , and τ_{aq} are shorter than the time scales that quantify the rate at which a newly formed spray droplet's temperature, radius, and salinity evolve. We therefore conclude that, following the assumptions herein, a model for spray-mediated air-sea gas exchange can assume that the gas concentration in spray droplets is always in instantaneous equilibrium with the local atmospheric gas concentration.

Keywords: sea spray; spume; jet drops; spray drops; gas exchange; gas transfer

1. Introduction

In the open ocean, when the wind blows strongly enough and long enough, the sea surface reaches a dynamic equilibrium where the work done by the wind on the sea is dissipated in part by breaking waves, which result in the formation of whitecaps (e.g., [1,2]). The bubbles and sea spray associated with breaking waves and their associated whitecaps enhance the air-sea exchange of heat, moisture, and gases [3]. However, not all bubbles upon bursting at the sea surface produce sea spray droplets [4], and not all sea spray droplets are formed by the bursting of whitecap bubbles (Figure 10 in reference [5]).

While many authors have assessed the role of sea spray droplets in the air-sea exchange of heat and moisture [6–10], Andreas and Monahan (2000) [11] gained further insights by looking at the role played by bubbles, and the moisture-laden air they contained, in the air-sea exchange of heat and moisture. Likewise, many research groups have considered the role of bubbles bursting on the sea surface in enhancing the air-sea exchange of a wide range of gases, particularly when the wind approaches speeds above 10 m s^{-1} [12–17]. Subsequently, many other researchers took up the study of bubble-mediated gas transfer [18–26]. Noting that the role of sea spray in gas transfer had not been assessed, our group was motivated to evaluate sea spray's potential role in addition to the established role of bubbles in this exchange.

A recent brief publication dealing with the time scales relevant to an evaluation of the role of sea spray droplets in air-sea gas exchange identified the importance of evaluating timescales involved in both droplet physics and gas diffusion [3]. Recognizing the benefits of a full systematic development of the time scales associated with the evolution of these droplets, and of the steps associated with gas moving into, and out of, these airborne droplets, we have undertaken to provide this comprehensive treatment in expanded form herein.

We therefore begin this formal treatment of how and whether sea spray might influence the rate of air-sea gas transfer following the approach that Andreas and colleagues used for assessing how sea spray affects air-sea heat and moisture transfer [9,27–31]. Microphysical modeling of the temperature and radius evolution of individual spray droplets underlies most of this work [32–35]. In turn, we will begin our study of spray-mediated gas transfer by first studying the microphysical, thermodynamic, and gas transfer properties of individual spray droplets. We quantify these processes with time scales that ultimately show us where the rate-limiting step is for spray-mediated gas transfer and, consequently, inform our decision on how next to proceed.

The difference in partial pressures of the gases in the sea and in the near-surface air (Δp) is dictated by a gas’s Henry’s Law Constant (K_H). In the case of sea spray, the dynamic nature of the evaporating droplet leads to a shifting K_H due to both changes in temperature and salinity. As wind speeds increase, the nature of sea spray also changes, shifting from small film droplets and moderate jet drops at wind speeds between 4 to 12 m s⁻¹ to a second sea spray source represented by the typically larger spume drops tearing off wave crests at higher wind speeds. The spume drops become increasingly important as wind speeds increase (>12 m s⁻¹). A critical analysis of the timescales involved in the gas exchange of sea spray involves the distinction between small droplets that remain in air long enough to reach equilibrium and large droplets that return to the sea before doing so, sometimes virtually unchanged. The former become hypersaline as they evaporate and dissolved gases experience a corresponding decrease in solubility and increase in partial pressure. The cutoff between the small and large droplet pools is greatly dependent on the relative humidity [26,36–38]. Ascertaining the fraction of sea spray that reaches equilibrium under a given set of conditions enables one to reasonably gauge the effusion of gas into the atmosphere from small drops. The larger drops will contribute to gas exchange primarily through changes in temperature and modest changes in volume. These interactions require accurate estimates of the timescales controlling gas transfer.

2. Theoretical Background

2.1. Spray Droplet Evolution

Microphysical modeling provides insights into spray droplet behavior [9,32,35,39], as shown in Figure 1 for a droplet whose initial radius (r_0) was 100 μm . Initially, droplet temperature (T) and radius (r) follow exponential relations:

$$\frac{T(t) - T_{eq}}{T_w - T_{eq}} = \exp(-t/\tau_T) \tag{1}$$

$$\frac{r(t) - r_{eq}}{r_0 - r_{eq}} = \exp(-t/\tau_r) \tag{2}$$

In Equations (1) and (2), t is the time since the droplet formed, T_w , the sea surface temperature (assumed to be the initial droplet temperature); T_{eq} and r_{eq} , the droplet’s equilibrium temperature and radius and τ_T and τ_r , the corresponding e-folding times to reach these equilibrium values.

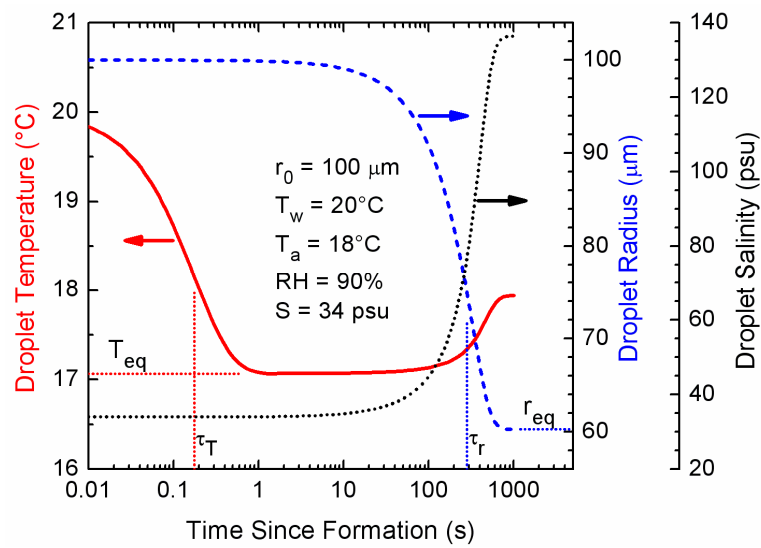


Figure 1. Results of a microphysical model [39] that predicts the temperature, radius, and salinity evolution of an individual spray droplet. This particular droplet formed with an initial radius of 100 μm (r_0) from surface seawater of 20 $^\circ\text{C}$ (T_w) and salinity 34 psu (S). It was thrown into air of temperature 18 $^\circ\text{C}$ (T_a) and relative humidity 90% (RH). The barometric pressure was 1000 mb. The T_{eq} , r_{eq} , τ_T , and τ_r are, respectively, the equilibrium temperature and radius and the e-folding times for the temperature and radius evolution.

The microphysical quantities T_{eq} , r_{eq} , τ_T , and τ_r all depend on the initial droplet radius, temperature, and salinity and on the environmental conditions like air temperature (T_a), relative humidity (RH), and barometric pressure. In particular, for droplets smaller than 100 μm , the curves in Figure 1 all shift to the left, i.e., to earlier times. For larger droplets, the curves all shift to the right, i.e., to later times. Nevertheless, for all radii, there is always the three-order-of-magnitude separation between τ_T and τ_r that Figure 1 depicts. These microphysical quantities are estimated using fast algorithms by Andreas (2005a).

Figure 2 shows the range of droplet sizes that we expect will be important for spray-mediated gas transfer, with sea spray droplets ranging in radius from 0.5 to 500 μm . This figure presents the spray generation function (F) as a volume flux. The number of droplets of radius r_0 produced per square meter of sea surface, per second, per micrometer increment in droplet radius is commonly denoted dF/dr_0 [5,28,40]. Therefore, the volume flux in Figure 2 is $(4\pi r_0^3/3)dF/dr_0$, for any spray-mediated process. Spume droplets carry most of the water and therefore, as with spray-mediated heat and moisture transfer [9,30]), may be responsible, under high-wind conditions, for most of the spray-mediated air-sea gas exchange. While the flux of smaller spray droplets, those produced by the bursting of whitecap bubbles varies as roughly the cube of the wind speed, it should be acknowledged that the wind dependence of the flux of the larger spume drops is not as well constrained.

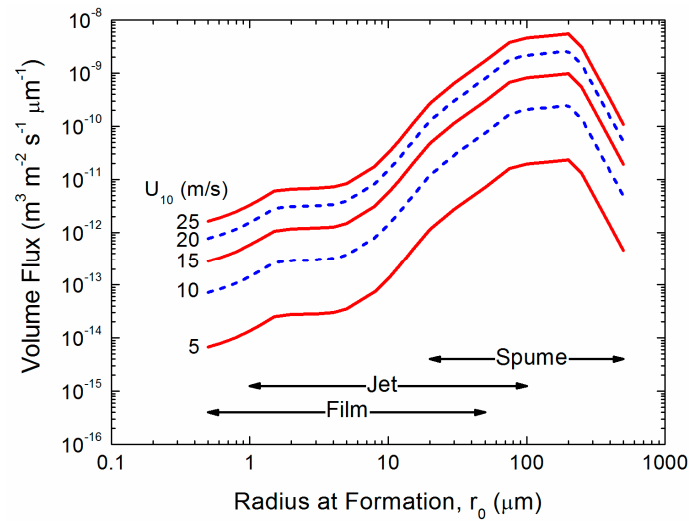


Figure 2. The spray generation function as a volume flux. Andreas [27] formed this function by smoothly joining the relation that Monahan et al. [41] deduced from spray created from bursting bubbles (film and jet droplets) with the relation from Fairall et al. [8], which is a reasonable function for the larger (spume) droplets [42].

2.2. Gases and Spray Droplets

The time scales that govern how gas molecules interact with water droplets are based on work by Seinfeld and Pandis [38], Pruppacher and Klett [43], and Lamb and Verlinde [44]. Consideration must be made, however, for differences wherein cloud droplets are often smaller than sea spray droplets, and are never as saline.

Figure 3 schematically shows how an individual spray droplet may exchange an arbitrary gas with an atmospheric reservoir. While gas exchange with cloud droplets is usually an invasion process, spray-mediated transfer, on the other hand, can involve both invasion due to changes in partial pressures and initial cooling of the droplet and evasion due to subsequent increases in temperature and evaporation. Though we hypothesize evasion will be the primary direction for spray-mediated air-sea gas transfer, both directions are addressed.

Gas transfer across an air-water interface is controlled by K_H where,

$$C_d(r_0) = K_H p_g(r_0) \tag{3}$$

Here, $p_g(r_0)$ is the partial pressure (or fugacity; Pilson 2013 [45], p. 416) of arbitrary gas g at the external surface of a droplet, and $C_d(r_0)$ is the concentration of the gas just inside the droplet. Here, p_g and C_d are in atm and mol L⁻¹, respectively. Hence, K_H has units of mol (L atm)⁻¹. Using the ideal gas law to convert p_g to the concentration of the gas in air (C_a). Equation (3) thus becomes

$$C_d(r_0) = K_H R T C_a(r_0) \tag{4}$$

where R (8.20574×10^{-2} atm L mol⁻¹ K⁻¹) is the universal gas constant, and T is in Kelvins. Note, the product $K_H R T$ is dimensionless. Equation (4) explains the apparent discontinuity in concentration in Figure 3 at the surface of the spray droplet.

For the gases of interest—helium, neon, argon, oxygen, nitrogen, and carbon dioxide— K_H generally increases with decreasing temperature and decreasing salinity. Therefore, in contrast to interfacial and bubble-mediated transfer, for which the ocean’s temperature and salinity and thus, K_H can be assumed to be constant during a gas flux measurement by eddy-covariance (i.e., for 30–60 min), the Henry’s law coefficient for an evolving spray droplet is continually changing. This may have important implications for measurements conducted in high-sea-spray conditions.

Figure 4 is an example of how K_H for each of our six gases would change during the droplet evolution that Figure 1 depicts. All K_H values increase slightly as the droplet initially cools; but if the droplet remains in the air long enough to reach radius equilibrium, its increasing salinity causes K_H to decrease to between 53% and 65% of its original value (see Appendix A). In other words, with time, a spray droplet generally becomes a less hospitable reservoir for dissolved gas, augmenting evasion.

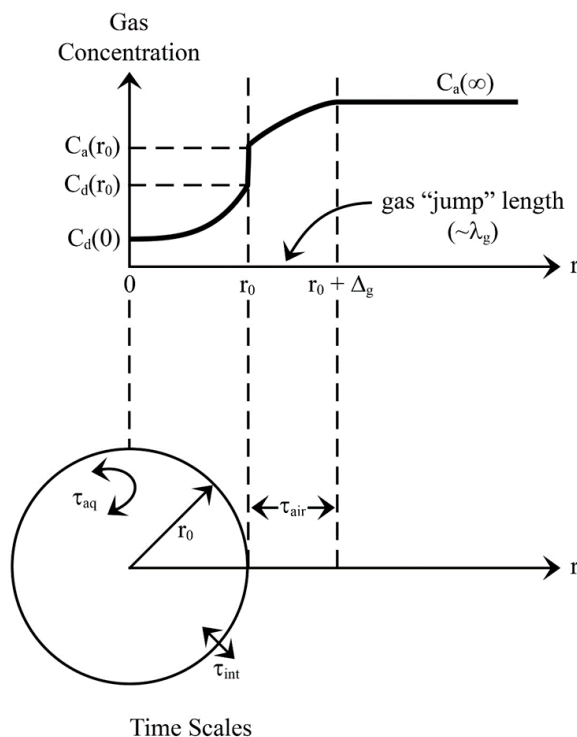


Figure 3. Gas invasion example. The upper part of the figure shows the gas concentration C as a function of radial distance r from the center of a spray droplet. The apparent discontinuity in concentration at r_0 is required by Henry’s law equilibrium. The lower part depicts the three time scales (τ_{air} , τ_{int} , τ_{aq}) defined in Section 2.3, relevant to spray-mediated gas exchange. Adapted from Seinfeld and Pandis (2006, p. 550) and Lamb and Verlinde (2011, p. 502).

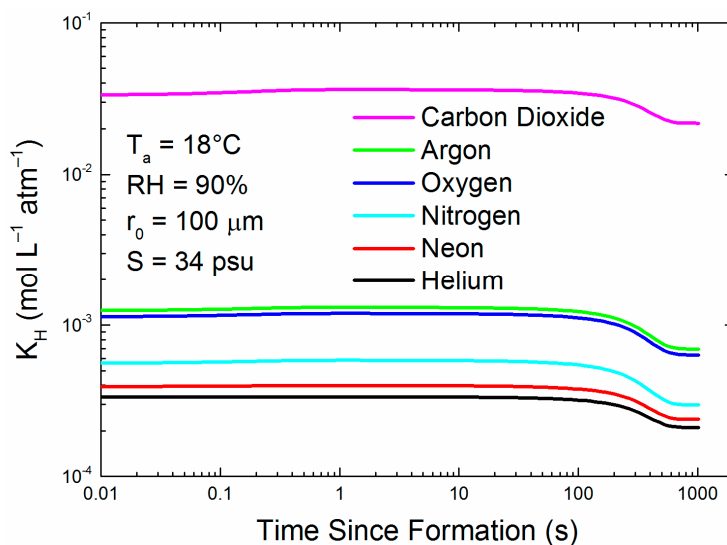


Figure 4. For each of the six gases, the figure shows how the Henry’s law coefficient changes for the evolving 100- μm droplet tracked in Figure 1.

2.3. Microphysics

Pruppacher and Klett ([43], p. 761) derive an equation for the rate of change of gas mass (m_g) in a solution droplet under the assumption that the gas in the droplet is well mixed:

$$\frac{dm_g}{dt} = 4\pi r(t)D'_g \left[\frac{C_d(t)}{K_H(t)RT_d(t)} - C_a(\infty) \right] \quad (5)$$

Here, t is time; the droplet's radius $r(t)$, gas concentration $C_d(t)$, and temperature $T_d(t)$ and the Henry's law coefficient $K_H(t)$ all depend on time. $C_a(\infty)$ is the gas concentration in air far from the droplet (Figure 3). D'_g is the modified diffusivity of the gas in air (cf. Andreas 1989, 2005b, [34,39]):

$$D'_g = \frac{D_g}{\frac{r}{r+\Delta_g} + \frac{D_g}{r\alpha} \left(\frac{2\pi M_g}{RT_a} \right)^{1/2}} \quad (6)$$

In this expression, D_g is the molecular diffusivity of the gas in air; M_g , the molecular weight of the gas; and T_a , the air temperature. Equation 6 incorporates two effects that dictate gas transfer to or from a small water droplet. The left term in the denominator accounts for surface curvature. If the droplet is small enough (i.e., $r < 10\Delta_g$) the air and gas may no longer behave as continuous fluids; the Δ_g , the gas "jump" length, which is approximately the mean free path of the gas in air (λ_g ; see Figure 3), determines what "small enough" is. Gas molecules cross this jump length as dictated by the kinetic theory of gases (e.g., [46], pp. 188, 234–235). Thus, in the second term in the denominator of (2.6), we recognize $(2\pi M_g/RT_a)^{1/2}$ as $4/\bar{v}_g$, where \bar{v}_g is the average speed of an ideal gas molecule according to the Maxwell-Boltzmann speed distribution ([46], pp. 60–64). Finally, in (2.6), α is the mass accommodation coefficient of the gas: the ratio of the number of gas molecules that stick to a droplet over the number that strike the droplet. Consequently, α must be one or less. There are few estimates of the value of α for our six gases. In his comparable microphysical model for heat and water vapor exchange with a spray droplet, Andreas [32,39]), used $\alpha_T = 0.7$ for heat exchange and a range of $\alpha_v = 0.036$ to 1.0 for water vapor [3]. The impact of α for each gas, is assessed through sensitivity calculations for a range of available values.

Recognizing in Equation (5) that $m_g = (4\pi r^3/3)C_d$, (5) becomes

$$\frac{dC_d}{dt} = -\frac{3D'_g}{r^2} \left(\frac{C_d}{K_HRT_d} - C_a \right) \quad (7)$$

Further, if we assume that r is the initial droplet radius r_0 and K_H and T_d are constant, (7) has the solution

$$C_d(t) = K_HRT_dC_a + (C_w - K_HRT_dC_a) \exp\left(\frac{-3D'_g t}{r_0^2 K_HRT_d}\right) \quad (8)$$

Here, C_w is the gas concentration in the surface seawater. Note, this assumes that the gas concentration in the droplet, C_d , is uniform. Note, T_d does change as the drop evolves, as does the radius; thus, K_H may change appreciably in saline droplets.

Equation (8) implies that gas concentration in the droplet evolves exponentially over an e-folding time identified with the subscript PK in Equation (9) because it is derived based on Pruppacher and Klett [43].

$$\tau_{PK} = \frac{r_0^2 K_HRT_d}{3D'_g} \quad (9)$$

But following Lamb and Verlinde ([44], p. 507), we recognize that τ_{PK} has two parts when we insert D'_g from (6):

$$\tau_{PK} = \frac{K_HRT_d}{3D_g} \left[\frac{r_0^3}{r_0 + \Delta_g} + \frac{D_g r_0}{\alpha} \left(\frac{2\pi M_g}{RT_a} \right)^{1/2} \right] \quad (10)$$

The first term dictates how rapidly gas molecules cross the jump layer and, therefore, is the time scale in air (see Figure 3):

$$\tau_{air,PK} = \frac{r_0^3 K_H R T_d}{3 D_g (r_0 + \Delta_g)} \tag{11}$$

The second term reflects the rate at which a droplet releases (or entrains) gas molecules across its interface and thus is the droplet’s interfacial time scale (again, see Figure 3):

$$\tau_{int,PK} = \frac{r_0 K_H R T_d}{3 \alpha} \left(\frac{2 \pi M_g}{R T_a} \right)^{1/2} \tag{12}$$

While Equations (11) and (12) are derived here following Lamb and Verlinde ([44] p. 507), who derive the same estimate as (12) for the interfacial time scale (i.e., $\tau_{int,LV} = \tau_{int,PK}$), they ignore the jump layer (and, thereby, [cf. (11)]).

$$\tau_{air,LV} = \frac{r_0^2 K_H R T_d}{3 D_g} \tag{13}$$

By assuming that the gas concentration at the external surface of the spray droplet is equal to that of the bulk air, Seinfeld and Pandis ([38], pp. 538, 549–551, 580–582) estimate the gas time scale in air as

$$\tau_{air,SP} = \frac{r_0^2}{4 D_g} \tag{14}$$

Following Kumar [47], Seinfeld and Pandis ([38], pp. 551–554) start with the equation for diffusion of gas within a spherical droplet:

$$\frac{dC_d}{dt} = D_{g,sw} \left(\frac{d^2 C_d}{dy^2} + \frac{2}{y} \frac{dC_d}{dy} \right) \tag{15}$$

Notice, in contrast to Pruppacher and Klett’s [43] derivation, C_d is now a function of radial position within the droplet. Here, also, $D_{g,sw}$ is the molecular diffusivity of a gas in seawater; and y is the radial distance from the center of the droplet, which is at $y = 0$. An assumed initial condition is, without losing generality, that at time zero, the initial droplet gas concentration $C_{d,t=0}$ is C_w .

$$C(y, t = 0) = C_w \text{ for } y \leq r_0 \tag{16}$$

A second boundary condition, because of the spherical symmetry, is that the droplet is well mixed, and at the center of the droplet ($y = 0$) and for all time t

$$\frac{dC_d}{dy} = 0 \tag{17}$$

The key part of this approach is identifying the flux boundary condition at the surface of the droplet. Here, the net flux across the droplet’s interface is (Seinfeld and Pandis [43], pp. 551–552; Lamb and Verlinde [44], pp. 503–504; cf. Bohren and Albrecht [46], pp. 233–234)

$$\phi_{net} = \frac{\alpha [C_a(r_0) - C_d(r_0)]}{K_H (2 \pi M_g R T_d)^{1/2}} \tag{18}$$

As Figure 3 implies, in this, $C_a(r_0)$ is the gas concentration at the surface of the droplet just outside of it; $C_d(r_0)$ is the gas concentration just inside the droplet.

Kumar [47] and Seinfeld and Pandis ([38], pp. 552–553) complete this analysis to derive the solution for the gas concentration within the droplet, which is, for $y \leq r_0$,

$$C_d(y, t) = C_a(r_0) \left[1 - \sum_{n=1}^{\infty} \frac{2r_0^2 H \sin(\beta_n y / r_0)}{y D_{g,sw} (L + L^2 + \beta_n^2) \sin(\beta_n)} \right] \exp\left(-\frac{\beta_n^2 D_{g,sw} t}{r_0^2}\right) \quad (19)$$

In this,

$$H = \frac{\alpha}{K_H (2\pi M_g R T_d)^{1/2}} \quad (20)$$

$$L = \frac{r_0 H}{D_{g,sw}} - 1 \quad (21)$$

and the β_n are the “ n ” positive roots of

$$\beta_n \cot(\beta_n) + L = 0 \quad (22)$$

We ultimately solve (22) by Newton’s method although Carslaw and Jaeger ([48], p. 492) tabulate β_n for $n = 1$ to 6. Kumar [47] and Seinfeld and Pandis ([38], p. 553), however, explain that just the first root, β_1 , provides an adequate solution in (19).

In (19), the e-folding time is

$$\tau_{aq,SP} = \frac{r_0^2}{\beta_1^2 D_{g,sw}} \quad (23)$$

For large values of L , nominally above 100, β_1 from (22) is π (e.g., Carslaw and Jaeger [29], p. 492) and

$$\lim_{L \rightarrow \infty} \tau_{aq,SP} = \frac{r_0^2}{\pi^2 D_{g,sw}} \quad (24)$$

We will see this case often in our subsequent calculations because L is large when r_0 is large, or the gas is not very soluble (i.e., a small K_H)—see (20) and (21). Of our six gases, all except carbon dioxide are weakly soluble.

This final time scale, τ_{aq} , quantifies mixing inside the aqueous solution droplet. The other two primary sources (Pruppacher and Klett [43], p. 764; Lamb and Verlinde [44], p. 508), likewise, arrive at the same estimate for this time scale, which we will therefore designate

$$\tau_{aq} = \frac{r_0^2}{\pi^2 D_{g,sw}} \quad (25)$$

Equation (25) “was derived” under the assumption that the fluid within the droplets is motionless; gas molecules thus would move only through molecular diffusion, $D_{g,sw}$. Ample evidence exists, however, that the fluid even in small droplets develops circulations when a shear stress occurs at the droplet’s surface (Clift et al. 1978, pp. 36–38, 127–129; Pruppacher and Klett [43], pp. 386–393). Consequently, mixing of the gas within a droplet is surely much faster than τ_{aq} suggests. We thus consider (25) as the lower limit for mixing of gas molecules within a spray droplet.

2.4. Droplet Residence Time

A droplet’s residence time in air is the boundary condition under which these processes are considered. A spray droplet can exchange heat, water vapor, and gases with air only during its (often brief) lifetime between creation and re-entry into the ocean. As spume droplets, which are formed by the wind tearing drops right off of the wave crests, accomplish most of the spray-mediated heat

and moisture exchange, Andreas and colleagues [9,28,30,31,49] based a residence time scale on their behavior where

$$\tau_f = \frac{h_{1/3}/2}{u_f(r_0)} \quad (26)$$

Here, $u_f(r_0)$ is the terminal fall velocity of droplets of radius r_0 . Also, $h_{1/3}$ is the significant wave height; consequently, $h_{1/3}/2$ ($\equiv A_{1/3}$) is the significant wave amplitude, the height above mean sea level where many spray droplets originate. $h_{1/3}$ can be taken from measurements; but in the absence of measurements of wave height, we estimate $h_{1/3}$ from Andreas and Wang's [50] algorithm in which $h_{1/3}$ goes as the square of the 10 m wind speed. Equation (26) models the residence time in air of a droplet that has reached terminal fall velocity. τ_f represents the minimum time aloft wherein droplets that have not reached terminal velocity would reside longer.

3. Spray Droplet Time Scales

Figure 5a–c compares time scales over a range of radii for one set of environmental conditions and for three gases: helium, oxygen, and carbon dioxide. In each plot, the τ_f , τ_r , and τ_T curves are the same, because these times do not depend on the gas. Helium ($M_g = 4$ g/mol), oxygen ($M_g = 32$ g/mol), and carbon dioxide ($M_g = 44$ g/mol) span the range from smallest to largest in our set of six gases, and thereby demonstrate how the size of the gas molecule influences τ_{air} , τ_{int} , and τ_{aq} . Any spray-mediated transfer, whether it is for sensible heat (τ_T), water vapor (τ_r), or gas molecules (τ_{air} , τ_{int} , τ_{aq}), must occur over a time less than the droplet's residence time, τ_f . This time scale decreases as the radius increases, because u_f increases with radius. The τ_f curves in Figure 5a–c are for a 10-m elevation wind speed of 12 m s^{-1} ; the τ_f curve will rise for increasing wind speed (because $h_{1/3}$ increases), allowing more spray-mediated exchange to take place. The τ_f curve, as an example, is above τ_r for radii up to about $30 \text{ }\mu\text{m}$. Droplets of $30 \text{ }\mu\text{m}$ and smaller thus can reach radius equilibrium and become more saline before they fall back into the ocean. Droplets larger than $30 \text{ }\mu\text{m}$, where $\tau_f < \tau_r$, on the other hand, fall back into the water before losing much water and, consequently, return to the ocean with approximately their original salinity. A droplet's temperature evolution is much faster. Thus, droplets up to about $200 \text{ }\mu\text{m}$ in radius have time to reach an equilibrium temperature of T_{eq} at this wind speed before they fall back into the sea.

Our several estimates of gas time scales are comparable to and even shorter than τ_T . The mixing of gas molecules within a spray droplet, parameterized as τ_{aq} is a maximum value that does not recognize any fluid motion in a spray droplet that could certainly enhance gas mixing by at least an order of magnitude. Consequently, we suspect that the true τ_{aq} will be at least ten times less than depicted.

Mixing within the droplets falls into two categories. (1) Small droplets in the film and jet droplet range for which mixing is primarily molecular that reach radial and temperature equilibrium while the droplets are airborne. The change in radius and consequent increase in salinity significantly alters the dissolved gas fugacity and drives evasion such that, it can be expected, the majority of the dissolved gas at the time of droplet formation is evaded and delivered to the atmosphere; and (2) The internal mixing in larger droplets of $r > 50 \text{ }\mu\text{m}$ needs careful consideration, as these droplets are more likely to return to the surface ocean before reaching radial equilibrium. There are few studies that address these larger droplet dynamics, and the majority of these are generated as spume droplets resulting from tearing off wave crests. There are, however, several analogous processes that have been evaluated in rain droplet studies ($50 < r < 2000 \text{ }\mu\text{m}$). As spume drops fall within this size range, the dynamics of raindrops may shed light on the internal mixing processes that apply to these large marine-derived droplets.

Drops for which $r < 500 \text{ }\mu\text{m}$ can be effectively treated as spheres that experience oscillations, which can be reasonably predicted from water surface tension and density. These oscillations introduce dynamic pumping or mixing of the gases in the droplet [51]. At drop radii above $500 \text{ }\mu\text{m}$, surface tension is overcome by weight force, and drop geometry deviates from the purely spherical. At $r > 500 \text{ }\mu\text{m}$ eddy shedding and sideways drift begins to occur [52] and collisions between large

drops add to the oscillations and further enhance these. Thus, these larger drops ($50 \mu\text{m} < r$) are turbulently mixed.

For the air time scales, τ_{air} , in Figure 5a–c we show only $\tau_{air,PK}$, (2.11), because it is near the Lamb and Verlinde [44] scale, (2.13), and because the Seinfeld and Pandis [38] scale, (2.14), is based (unrealistically) only on molecular diffusion of gas molecules to and from a spray droplet. Note that $\tau_{air,PK}$ is orders of magnitude less than τ_T , which we consider to represent very fast exchange. $\tau_{air,PK}$ does, however, increase by roughly three orders of magnitude between helium and carbon dioxide as a consequence of how increasing molecular weight slows molecular velocities in air. The final time scale shown in Figure 5a–c quantifies exchange across a droplet’s interface, and we represent this exchange with $\tau_{int,PK}$, (2.12), which, although increasing with the increasing molecular weight of the gas molecule, always represents extremely fast gas transfer.

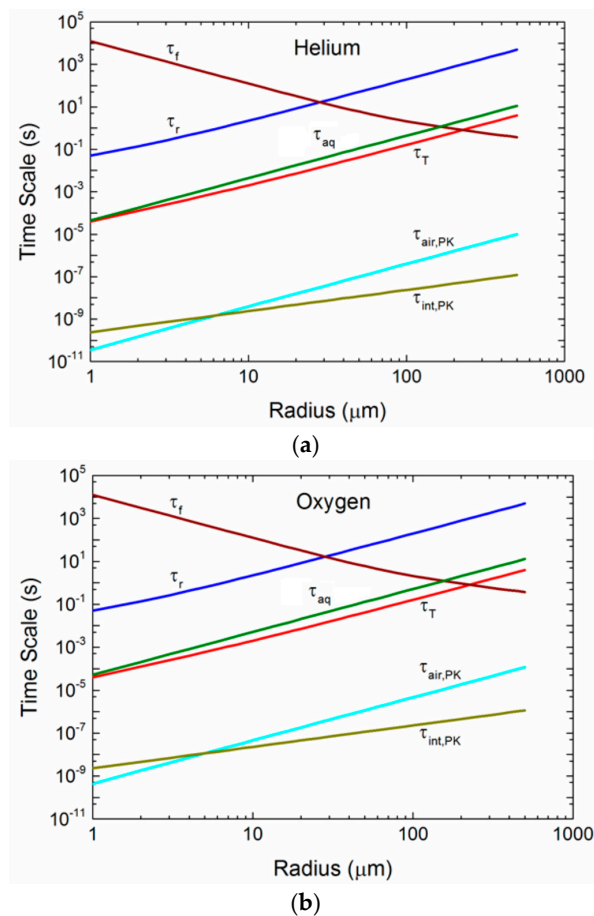


Figure 5. Cont.

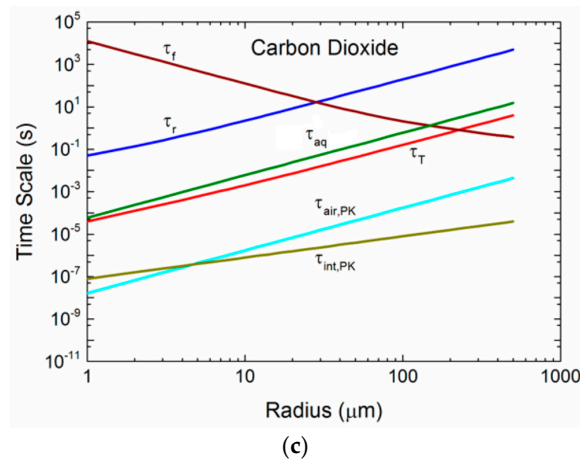


Figure 5. (a) For droplets of radius r_0 , the figure shows the microphysical time scales for temperature (τ_T) and radius (τ_r) evolution, the droplet residence time (τ_f), and the time scales that govern transfer of helium molecules to or from a spray droplet in air (τ_{air}), across the air-droplet interface (τ_{int}), and within the droplet (τ_{aq}). The interfacial time scale derives from both Pruppacher and Klett ([43]; $\tau_{int,PK}$), Equation (2.11), and Seinfeld and Pandis ([38]; $\tau_{int,SP}$), Equation (2.23). The time scale in air derives from Pruppacher and Klett ($\tau_{air,PK}$), Equation (2.10); and the aqueous mixing time scale (τ_{aq}) is (2.25). Conditions here are for a 10-m wind speed of 12 m s^{-1} , air temperature and water temperature of $20 \text{ }^\circ\text{C}$, relative humidity of 85%, and sea surface salinity of 34 psu; the mass accommodation coefficient is set at $\alpha = 0.036$. For this value, β_1 in Seinfeld and Pandis’s $\tau_{int,SP}$ is π , and $\tau_{int,SP}$ is the same as τ_{aq} (from [3]); (b) for oxygen; (c) for carbon dioxide (from [3]).

Figure 6 shows the range of $\tau_{air,PK}$ values for our six gases. As with Figure 5a–c, $\tau_{air,PK}$ increases monotonically with the molecular weight of the gas. In effect, the mean molecular speed predicted by the kinetic theory of gases decreases as the molecular weight increases (see (Equation (12))). Still, all our gases of interest can cross the jump layer well within the time granted by a droplet’s flight from creation and back to the sea surface. Note that τ_f in Figure 6 is based on a wind speed of 12 m s^{-1} ; at higher wind speeds, when spray concentrations would rapidly increase, τ_f gets longer with the square of the wind speed.

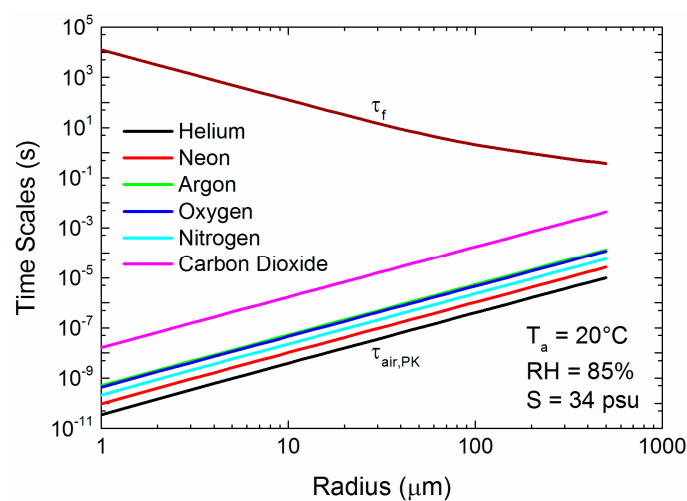


Figure 6. The time scale that governs gas transfer between the ambient air and the surface of a spray droplet derived from Pruppacher and Klett’s [43] approach, $\tau_{air,PK}$, (2.11), for six different gases. The plot also shows the residence τ_f for a 10-m wind speed of 12 m s^{-1} . Air (T_a) and water temperature are assumed to be $20 \text{ }^\circ\text{C}$, relative humidity (RH) is 85%, and sea surface salinity (S) is 34 PSU.

3.1. Implications of the Time Scales

Our comparisons of the time scales τ_{air} , τ_{int} , and τ_{aq} in Figure 5a–c yield significantly different results based on the approach of choice. The time for gas molecules to transit the jump layer that we base on Pruppacher and Klett’s [43] approach (i.e., $\tau_{air,PK}$) is so short that we could assume the gas concentration right at the exterior surface of a spray droplet is always $C_a(\infty)$. Pruppacher and Klett’s approach also yields an interfacial time scale ($\tau_{int,PK}$) that is even shorter for most droplet sizes. The caveat, though, is that their approach assumes that the gas is well mixed inside the droplets. Because our estimate of this internal mixing time scale, τ_{aq} , is orders of magnitude longer than $\tau_{int,PK}$, this assumption seems inappropriate. We have discussed how, because of fluid motion within spray droplets, the actual time scale for internal mixing will be shorter than τ_{aq} , but we are uncertain whether it will be the 4 orders of magnitude shorter that would be necessary to justify Pruppacher and Klett’s approach.

At this point, it appears essential that we make at least a crude estimate of how fluid motion within spray droplets may affect τ_{aq} . LeClair et al. ([53]; also [54], pp. 127–129; [43], pp. 386–393) report observations and theoretical predictions for the surface velocity (v_s) inside droplets in a shear flow. That shear flow generally is a consequence of the droplet’s falling at terminal velocity (u_f). The ratio v_s/u_f is predicted to be a function of the droplet Reynolds number, $Re = 2r_0u_f/\nu$, where ν is the kinematic viscosity of air.

Table 1 shows our estimates of v_s for a range of droplet sizes. A reasonable method for estimating the effect of fluid motion within a droplet is to calculate a motion-induced diffusivity as $r_0 v_s$ (e.g., [55], pp. 8–11). Table 1 also shows this estimate, which ranges from $1.2 \times 10^{-12} \text{ m}^2 \text{ s}^{-1}$ for 1 μm droplets to $8.0 \times 10^{-5} \text{ m}^2 \text{ s}^{-1}$ for our largest droplets (500 μm). For comparison, the molecular diffusivities at 20 °C for our gases of interest range from $1.7 \times 10^{-9} \text{ m}^2 \text{ s}^{-1}$ for carbon dioxide to $2.3 \times 10^{-9} \text{ m}^2 \text{ s}^{-1}$ for helium. That is, for all but the smallest droplets that we are considering, fluid motion within the droplets could increase the effective gas diffusivity by several orders of magnitude.

Table 1. Estimated effects of fluid motion on enhancing mixing within spray droplets. The $r_0 v_s$ is the estimate of the motion-induced diffusion within a spray droplet of the given radius. Compare these values with $D_{g,sw}$, which ranges from 1.7×10^{-9} to $2.3 \times 10^{-9} \text{ m}^2 \text{ s}^{-1}$ for our six gases. In Re , the viscosity of air is calculated at 20 °C and is $1.504 \times 10^{-5} \text{ m}^2 \text{ s}^{-1}$.

r_0 (μm)	u_f (m s^{-1})	Re	v_s/u_f ^a	v_s (m s^{-1})	$r_0 v_s$ ($\text{m}^2 \text{ s}^{-1}$)
1	1.2×10^{-4}	1.6×10^{-5}	0.01	1.2×10^{-6}	1.2×10^{-12}
10	0.123	0.0164	0.01	1.2×10^{-4}	1.2×10^{-9}
50	0.254	1.69	0.012	3.1×10^{-3}	1.9×10^{-7}
100	0.725	9.65	0.016	0.012	1.2×10^{-6}
200	1.67	44.4	0.024	0.030	1.0×10^{-5}
500	4.10	272	0.042	0.16	1.0×10^{-5}

^a Estimated from Table 6 and Figure 7 in LeClair et al. (1972).

As just one sensitivity calculation to demonstrate this effect, we repeat in Figure 7 our time scales for carbon dioxide from Figure 5c, but here increase the molecular diffusivity in seawater, $D_{g,sw}$, by a factor of 10. We also show τ_f for a 10-m elevation wind speed of 20 m s^{-1} . Increasing the effective diffusivity of carbon dioxide within spray droplets by a factor of 10 decreases τ_{aq} by a factor of 10. As a result, for $U_{10} = 12 \text{ m s}^{-1}$, the τ_f crossover with the τ_{aq} curve increases from a radius of about 150 μm to over 300 μm ; more large droplets become involved in the gas transfer. For a wind speed of 20 m s^{-1} , the crossover moves out to r_0 of 400 μm . Even more large droplets participate fully in spray-mediated gas transfer with increasing wind speed. Furthermore, if we interpret Table 1 literally, it suggests that, because $r_0 v_s$ increases with increasing droplet radius, internal mixing (τ_{aq}) is even more efficient than in Figure 7 with its enhanced internal mixing ($10 D_{g,sw}$). In other words, the τ_{aq}

curve would fall farther below the τ_f curve at a larger radius than Figure 7 depicts. Our results also indicate that the choice of a mass accommodation coefficient within reasonable limits ($0.01 \leq \alpha \leq 1.0$) does not alter our conclusions about how sea spray mediates gas transfer, at least for our six gases of interest.

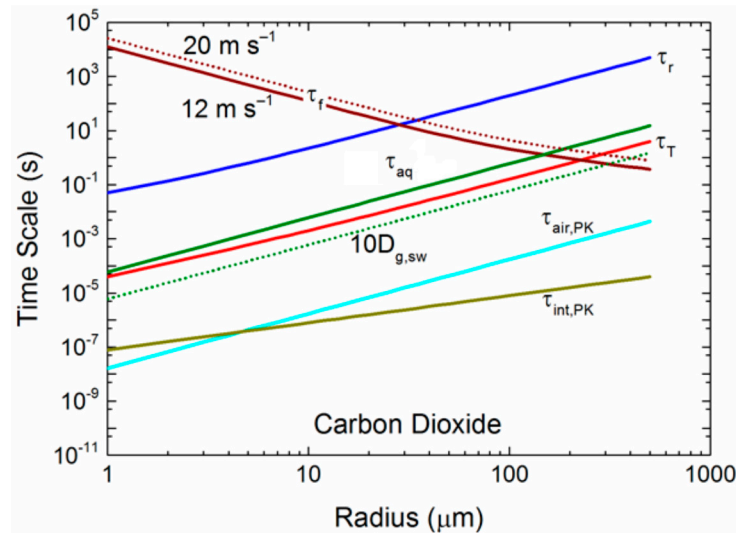


Figure 7. The dashed green curve gives τ_{aq} when we increase the diffusivity within the droplets from 5 c to $10D_{g,sw}$. The dashed τ_f curve gives the residence time for a 10-m wind speed of 20 m s^{-1} .

Consequently, a conceptual picture is emerging from this discussion in which gas transfer in each of the three potential rate-limiting steps is so fast that the gas in ambient air can almost always be assumed to be in instantaneous equilibrium with the evolving spray droplet. Only for the largest radii and for weak to moderate winds, say less than 15 m s^{-1} , may droplets fall back into the ocean before establishing equilibrium with the atmospheric gas reservoir.

3.2. Initial Gas Concentration in Spray Droplets

Our implicit assumption throughout has been that spray droplets are created with the same gas concentration as the near-surface ocean, C_w . For spume droplets, which form at the crests of breaking waves where turbulence in the seawater produces effective vertical mixing, this assumption is a good one. It should be noted that gas transfer for spume droplets returning to the sea can be in either direction and is primarily controlled by the temperature differential between air and sea. In cases where air temperature is lower than the sea temperature, net cooling of the spume aqueous phase results, thereby reducing the fugacity of a dissolved gas in spume. This leads to gas retention or, where the partial pressure of the gas in air is sufficiently high, gas invasion from the atmosphere to the droplet. That is, cooled spume drops may act as sinks for atmospheric gases or as attenuators that dampen biogenic gases such as DMS derived in the sea.

For the jet and film droplets that derive from bursting bubbles, however, we need to look more closely at this assumption. In terms of gas transfer at the air-sea interface, all six of our gases are controlled by flow through a diffusive sublayer on the water side of the interface [56,57]. The gas concentration changes through this sublayer from C_w , the concentration in bulk seawater at the bottom of the layer, to $C_a(\infty)$, the concentration in the ambient air at the top of the layer. Broecker and Peng [58] estimate the thickness of this sublayer as being between about 100 and 300 μm .

The bubbles that produce jet and film droplets most often have diameters less than 300 μm [42], and would thus burst from within this aqueous sublayer where the gas concentration in the water is somewhere between C_w and $C_a(\infty)$. Because the water entrained into jet droplets comes primarily from concentric spherical shells beginning with one corresponding to the interior surface of the parent

bubble [59], jet droplets should have gas concentrations nearer to C_w than to $C_a(\infty)$. For bubbles larger than 300 μm in diameter, it is reasonable to assume that droplets (primarily spume) carry gas concentrations of C_w .

Film droplets, on the other hand, derive from the bubble cap, which is a thin film over the bubble at the air-sea interface. That film cap can be of order of 1 μm thick and is, therefore, not much of a barrier for gas transfer between the air in the bubble and the ambient air. We thus expect that the gas concentration in the film droplets, which derive from this bubble cap, will be near $K_H C_a(\infty)$ or equilibrated to the bubble air. Film droplets may thus play little role in mediating air-sea gas transfer of the gases considered here, though they may be important in the gas exchange of biogenic gases concentrated in the surface films.

3.3. Surface-Active Material

Surface-active material—primarily organic—that is known to collect on bubbles as they rise in the water column and to form as monolayers on the sea surface [60–63] can be entrained onto spray droplets and, thus, affect their chemical and physical properties. Such contamination could affect several aspects of what we are assuming about spray droplets and the time scales that we have been discussing.

For example, a contaminated surface will retard evaporation from a spray droplet, and thus lengthen τ_r . Surface contamination can also cause a spherical liquid droplet to behave more like a rigid sphere ([64], p. 237; [54], p. 125), thereby lowering the drag coefficient (e.g., Pruppacher and Klett [43], pp. 382, 385–386; [54], pp. 129–131). Alternately, the surface may experience more drag due to irregularities.

Surface contamination alters the drag coefficient of droplets by changing—generally slowing—their internal circulation. Consequently, the internal mixing time scale for a droplet would not be a small fraction of τ_{aq} , as we had earlier explained, but would, with surface contamination, be pushed back toward τ_{aq} . In other words, the diffusion of a gas within a spray droplet would slow if the surface were contaminated, but the time scale would still be no longer than τ_{aq} , (2.25).

A last effect of surface contamination on a spray droplet would be to its surface tension. Surface-active material tends to lower the surface tension of water (Pruppacher and Klett [43], p. 130). Lower surface tension means droplets have less tendency to be spherical; they therefore become more susceptible to breakup. The ultimate result is that the near-surface droplet size distribution may shift to smaller droplets [65].

4. Conclusions

Sea spray gas diffusion follows a series of steps, including (1) diffusion between the deep interior of the droplet and its interior surface, (2) diffusion across the air-droplet interface, and (3) diffusion between the air-side boundary layer and the bulk atmosphere. If a gas undergoes a series of reactions while dissolved in sea spray, such as in the case of CO_2 , then (4) the timescales of these kinetics are also important. Of the six gases, 5 can be described by the non-reactive timescales 1 to 3. Only carbon dioxide participates in the additional fourth step, and these timescales will be considered in future work.

This comprehensive analysis confirms that, regardless of the model, the diffusional timescales occur at significantly faster timescales than the rates of droplet temperature and radius change. It is therefore possible to proceed with a sea-spray gas-exchange model that assumes that these latter rate-limiting steps control gas transfer. Although, for “clean” sea spray, the interfacial diffusion was not rate limiting, it is important to consider the effects on diffusion rates for sea spray that contains biogenic surfactants to establish thresholds that may impede diffusion.

Acknowledgments: We dedicate this manuscript to our late colleague Edgar L. Andreas, who catalyzed this work. We thank Stephen E. Schwartz for a helpful discussion on the mass accommodation coefficient, and Emily Moynihan of Blythe Visual for preparing Figures 1, 4 and 5. The National Science Foundation supported this work with awards 13-56377 (ELA) and 13-56541 (PV and ECM).

Author Contributions: The earliest draft of this paper was initiated by E.L.A., with contributions from P.V. and E.C.M. Subsequent to the death of E.L.A., the surviving authors, P.V. and E.C.M., jointly wrote the several following, expanded, drafts of this paper, and are jointly responsible for the finished manuscript. This paper, dealing solely with concepts and theory, involved no new field measurements or laboratory experiments.

Conflicts of Interest: The authors declare no conflict of interest.

Appendix A. Evaluating the Henry's Law Coefficient, K_H

Our emphasis here is on the six most abundant atmospheric gases: helium, neon, argon, oxygen, nitrogen, and carbon dioxide. We base our calculations of the Henry's law coefficient for these on the analyses by Weiss (1970, 1971, 1974 [66–68]; cf. Broecker and Peng 1982, Table 3-1 [69]; Wanninkhof 1992 [70]; Millero 2001, Table 5.4 [71]; Pilson 2013 [45], p. 418). Only for carbon dioxide, however, did Weiss (1974) express the solubility in terms of the Henry's law coefficient; for carbon dioxide, we therefore use Weiss's equation as written.

For helium, neon, argon, oxygen, and nitrogen, Weiss (1970, 1971 [66,67]) reported the Bunsen solubility β . Because the Bunsen coefficient is defined as the volume of gas dissolved in a given volume of solvent at standard temperature and pressure (Pilson 2013 [45], pp. 416–418), β and K_H are related by

$$\beta = K_H RT \left(\frac{T_K}{T} \right) \quad (\text{A1})$$

Here, R is again the universal gas constant, $T_K = 273.15$ K, and T is the actual Kelvin temperature. β , K_H , R , T , and T_K/T are all dimensionless in our preferred system of units.

Weiss's (1970, 1971 [66,67]) equations all predict $\ln[\beta(T,S)]$ as functions of temperature (T) and salinity (S). To use these to calculate K_H , we simply rearrange (A1) as

$$\ln[K_H(T, S)] = \ln[\beta(T, S)] - \ln(RT) - \ln(T_K/T) \quad (\text{A2})$$

and use Weiss's equation directly to calculate $\ln[\beta(T,S)]$.

References

1. Monahan, E.C.; MacNiocaill, G. (Eds.) *Oceanic Whitecaps and Their Role in Air-Sea Exchange Processes*; Springer: Dordrecht, The Netherlands, 1986; 294p.
2. Bortkovskii, R.S. *Air-Sea Exchange of Heat and Moisture during Storms*; Springer: Dordrecht, The Netherlands, 1987; 194p.
3. Andreas, E.L.; Vlahos, P.; Monahan, E.C. The potential role of sea spray droplets in facilitating air-sea gas transfer. *IOP Conf. Ser. Earth Environ. Sci.* **2016**, *35*, 012003. [[CrossRef](#)]
4. Blanchard, D.C. The electrification of the atmosphere by particles from bubbles in the sea. *Prog. Oceanogr.* **1963**, *1*, 71–202. [[CrossRef](#)]
5. Monahan, E.C.; Spiel, D.E.; Davidson, K.L. A model of marine aerosol generation via whitecaps and wave disruption. In *Oceanic Whitecaps and Their Role in Air-Sea Exchange Processes*; Monahan, E.C., MacNiocaill, G., Eds.; D. Reidel: Dordrecht, The Netherlands, 1986; pp. 167–174.
6. Borisenkov, E.P. Some mechanisms of atmosphere-ocean interaction under stormy weather conditions. *Probl. Arct. Antart* **1974**, *43–44*, 330–347.
7. Mestayer, P.G.; Lefauconnier, C. Spray droplet generation, transport, and evaporation in a wind wave tunnel during the Humidity over the Sea Experiments in the Simulation Tunnel. *J. Geophys. Res.* **1988**, *93*, 572–586. [[CrossRef](#)]
8. Fairall, C.W.; Kepert, J.D.; Holland, G.J. The effect of sea spray on surface energy transports over the ocean. *Glob. Atmos. Ocean Syst.* **1994**, *2*, 121–142.

9. Andreas, E.L. Sea spray and the turbulent air-sea heat fluxes. *J. Geophys. Res.* **1992**, *97*, 11429–11441. [[CrossRef](#)]
10. Edson, J.B.; Anquetin, S.; Mestayer, P.G.; Sini, J.F. Spray droplet modeling: 2. An interactive eulerian-lagrangian model of evaporating spray droplets. *J. Geophys. Res.* **1996**, *101*, 1279–1293. [[CrossRef](#)]
11. Andreas, E.L.; Monahan, E.C. The role of whitecap bubbles in air-sea heat and moisture exchange. *J. Phys. Oceanogr.* **2000**, *30*, 433–442. [[CrossRef](#)]
12. Atkinson, L.P. Effect of air bubble solution on air-sea gas exchange. *J. Geophys. Res.* **1973**, *78*, 962–968. [[CrossRef](#)]
13. Thorpe, S.A. On the clouds of bubbles formed by breaking wind waves in deep water and their role in air-sea gas transfer. *Philos. Trans. R. Soc. Lond. A* **1982**, *304*, 155–210. [[CrossRef](#)]
14. Merlivat, L.; Memery, L. Gas exchange across an air-water interface: Experimental results and modeling of bubble contribution to transfer. *J. Geophys. Res.* **1983**, *88*, 707–724. [[CrossRef](#)]
15. Monahan, E.C.; Spillane, M.C. The role of oceanic whitecaps in air-sea gas exchange. In *Gas Transfer at Water Surfaces*; Brutsaert, W., Jirka, G.J., Eds.; D. Reidel: Dordrecht, The Netherlands, 1984; pp. 495–503.
16. Memery, L.; Merlivat, L. Modelling of gas flux through bubbles at the air-water interface. *Tellus B Chem. Phys. Meteorol.* **1985**, *37*, 272–285. [[CrossRef](#)]
17. Liss, P.S.; Merlivat, L. Air-sea gas exchange rates: Introduction and synthesis. In *The Role of Air-Sea Exchange in Geochemical Cycling*; Buat-Ménard, P., Ed.; D. Reidel: Dordrecht, The Netherlands; Lancaster, UK, 1986; pp. 113–127.
18. Woolf, D.K.; Thorpe, S.A. Bubbles and the air-sea exchange of gases in near-saturation conditions. *J. Mar. Res.* **1991**, *49*, 435–466. [[CrossRef](#)]
19. Wallace, D.W.R.; Wirick, C.D. Large air-sea gas fluxes associated with breaking waves. *Nature* **1992**, *356*, 694–696. [[CrossRef](#)]
20. Keeling, R.F. On the role of large bubbles in air-sea gas exchange and supersaturation in the ocean. *J. Mar. Res.* **1993**, *51*, 237–271. [[CrossRef](#)]
21. Woolf, D.K. Bubbles and the air-sea transfer velocity of gases. *Atmos. Ocean* **1993**, *31*, 517–540. [[CrossRef](#)]
22. Asher, W.E.; Wanninkhof, R. The effect of bubble-mediated gas transfer on purposeful dual-tracer gaseous transfer experiments. *J. Geophys. Res.* **1998**, *103*, 10555–10560. [[CrossRef](#)]
23. Asher, W.E.; Karle, L.M.; Higgins, B.J.; Farley, P.J.; Monahan, E.C.; Leifer, I.S. The influence of bubble plumes on air-seawater gas transfer velocities. *J. Geophys. Res. Oceans* **1996**, *101*, 12027–12041. [[CrossRef](#)]
24. Monahan, E.C. The physical and practical implications of a CO₂ gas transfer coefficient that varies as the cube of the wind speed. In *Gas Transfer at Water Surfaces*; Donelan, M.A., Drennan, W.M., Saltzman, E.S., Wanninkhof, R., Eds.; American Geophysical Union: Washington, DC, USA, 2002; pp. 193–197.
25. Vlahos, P.; Monahan, E.C. A generalized model for the air-sea transfer of dimethyl sulfide at high wind speeds. *Geophys. Res. Lett.* **2009**, *36*, L21605. [[CrossRef](#)]
26. Vlahos, P.; Monahan, E.C.; Huebert, B.J.; Edson, J.B. Wind-dependence of DMS transfer velocity: Comparison of model with Southern Ocean observations. In *Gas Transfer at Water Surfaces 2010*; Komori, S., McGillis, W.R., Kurose, R., Eds.; Kyoto University Press: Kyoto, Japan, 2011; pp. 455–463.
27. Andreas, E.L. Spray-mediated enthalpy flux to the atmosphere and salt flux to the ocean in high winds. *J. Phys. Oceanogr.* **2010**, *40*, 608–619. [[CrossRef](#)]
28. Andreas, E.L.; DeCosmo, J. The signature of sea spray in the HEXOS turbulent heat flux data. *Bound. Layer Meteorol.* **2002**, *103*, 303–333. [[CrossRef](#)]
29. Andreas, E.L.; Edson, J.B.; Monahan, E.C.; Rouault, M.P.; Smith, S.D. The spray contribution to net evaporation from the sea: A review of recent progress. *Bound. Layer Meteorol.* **1995**, *72*, 3–52. [[CrossRef](#)]
30. Andreas, E.L.; Persson, P.O.G.; Hare, J.E. A bulk turbulent air-sea flux algorithm for high-wind, spray conditions. *J. Phys. Oceanogr.* **2008**, *38*, 1581–1596. [[CrossRef](#)]
31. Andreas, E.L.; Mahrt, L.; Vickers, D. An improved bulk air-sea surface flux algorithm, including spray-mediated transfer. *Q. J. R. Meteorol. Soc.* **2015**, *141*, 642–654. [[CrossRef](#)]
32. Andreas, E.L. Time constants for the evolution of sea spray droplets. *Tellus B* **1990**, *42*, 481–497. [[CrossRef](#)]
33. Andreas, E.L. Approximation formulas for the microphysical properties of saline droplets. *Atmos. Res.* **2005**, *75*, 323–345. [[CrossRef](#)]

34. Andreas, E.L. *Handbook of Physical Constants and Functions for Use in Atmospheric Boundary Layer Studies*; ERDC/CRREL Monograph M-05-1; U.S. Army Cold Regions Research and Engineering Laboratory: Hanover, NH, USA, 2005; 42p.
35. Andreas, E.L.; DeCosmo, J. Sea spray production and influence on air-sea heat and moisture fluxes over the open ocean. In *Air-Sea Exchange: Physics, Chemistry and Dynamics*; Geernaert, G.L., Ed.; Kluwer: Alphen aan den Rijn, The Netherlands, 1999; pp. 327–362.
36. Twomey, S. The identification of individual hygroscopic particles in the atmosphere by a phase-transition method. *J. Appl. Phys.* **1953**, *24*, 1099–1102. [[CrossRef](#)]
37. Tang, I.N.; Munkelwitz, H.R. Composition and temperature dependence of the deliquescence properties of hygroscopic aerosols. *Atmos. Environ. Part A Gen. Top.* **1993**, *27*, 467–473. [[CrossRef](#)]
38. Seinfeld, J.H.; Pandis, S.N. *Atmospheric Chemistry and Physics: From Air Pollution to Climate Change*, 2nd ed.; John Wiley and Sons: Hoboken, NJ, USA, 2006; 1203p.
39. Andreas, E.L. *Thermal and Size Evolution of Sea Spray Droplets*; CRREL Rep. 89-11; U.S. Army Cold Regions Research and Engineering Laboratory: Hanover, NH, USA, 1989; 37p.
40. Smith, M.H.; Park, P.M.; Consterdine, I.E. Marine aerosol concentrations and estimated fluxes over the sea. *Q. J. R. Meteorol. Soc.* **1993**, *119*, 809–824. [[CrossRef](#)]
41. Monahan, E.C. The ocean as a source of atmospheric particles. In *The Role of Air-Sea Exchange in Geochemical Cycling*; Buat-Menard, P., Ed.; Springer: Dordrecht, The Netherlands, 1986; pp. 129–163.
42. Andreas, E.L. Andreas, E.L. A review of the sea spray generation function for the open ocean. In *Atmosphere-Ocean Interactions*; Perrie, W., Ed.; WIT Press: Ashurst, UK, 2002; Volume 1, pp. 1–46.
43. Pruppacher, H.R.; Klett, J.D. *Microphysics of Clouds and Precipitation, 2nd Revised ed.*; Springer: Dordrecht, The Netherlands, 2010; 954p.
44. Lamb, D.; Verlinde, J. *Physics and Chemistry of Clouds*; Cambridge University Press: Cambridge, UK, 2011; 584p.
45. Pilson, M.E.Q. *An Introduction to the Chemistry of the Sea*, 2nd ed.; Cambridge University Press: Cambridge, UK, 2013; 524p.
46. Bohren, C.F.; Albrecht, B.A. *Atmospheric Thermodynamics*; Oxford University Press: Oxford, UK, 1998; 402p.
47. Kumar, S. The characteristic time to achieve interfacial phase equilibrium in cloud drops. *Atmos. Environ.* **1989**, *23*, 2299–2304. [[CrossRef](#)]
48. Carslaw, H.S.; Jaeger, J.C. *Conduction of Heat in Solids*, 2nd ed.; Oxford University Press: Oxford, UK, 1996; 510p.
49. Mestayer, P.G.; Van Eijk, A.M.J.; de Leeuw, G.; Tranchant, B. Numerical simulation of the dynamics of sea spray over the waves. *J. Geophys. Res.* **1996**, *101*, 20771–20797. [[CrossRef](#)]
50. Andreas, E.L.; Wang, S. Predicting significant wave height off the northeast coast of the United States. *Ocean Eng.* **2007**, *34*, 1328–1335. [[CrossRef](#)]
51. Szakall, M.; Mitra, S.K.; Diehl, K.; Borrmann, S. Shapes and oscillations of falling raindrops—A review. *Atmos. Res.* **2010**, *97*, 416–425. [[CrossRef](#)]
52. Beard, K.V.; Kubesh, R.J.; Ochs, H.T. Laboratory measurements of small raindrop distortion. Part I: Axis ratios and fall behavior. *J. Atmos. Sci.* **1991**, *48*, 698–710. [[CrossRef](#)]
53. LeClair, B.P.; Hamielec, A.E.; Pruppacher, H.R.; Hall, W.D. A theoretical and experimental study of the internal circulation in water drops falling at terminal velocity in air. *J. Atmos. Sci.* **1972**, *29*, 728–740. [[CrossRef](#)]
54. Clift, R.; Grace, J.; Weber, M.E. *Bubbles, Drops, and Particles*; Dover: Mineola, NY, USA, 1978; 381p.
55. Tennekes, H.; Lumley, J.L. *A First Course in Turbulence*; MIT Press: Cambridge, MA, USA, 1972; 300p.
56. Liss, P.S. Gas transfer: Experiments and geochemical implications. In *Air-Sea Exchange of Gases and Particles*; Liss, P.S., Slinn, W.G.N., Eds.; D. Reidel: Dordrecht, The Netherlands, 1983; pp. 241–298.
57. Donelan, M.A.; Wanninkhof, R. Gas transfer at water surfaces—Concepts and issues. In *Gas Transfer at Water Surfaces*; Donelan, M.A., Drennan, W.M., Saltzman, E.S., Wanninkhof, R., Eds.; American Geophysical Union: Washington, DC, USA, 2002; pp. 1–10.
58. Broecker, W.S.; Peng, T.-H. Gas exchange rates between air and sea. *Tellus* **1974**, *26*, 21–35. [[CrossRef](#)]
59. MacIntyre, F. Flow patterns in breaking bubbles. *J. Geophys. Res.* **1972**, *77*, 5211–5228. [[CrossRef](#)]
60. MacIntyre, F. The top millimeter of the ocean. *Sci. Am.* **1974**, *230*, 62–77. [[CrossRef](#)]

61. Blanchard, D.C. The ejection of drops from the sea and their enrichment with bacteria and other materials: A review. *Estuaries* **1989**, *12*, 127–137. [[CrossRef](#)]
62. Blanchard, D.C. Surface-active monolayers, bubbles, and jet drops. *Tellus B* **1990**, *42*, 200–205. [[CrossRef](#)]
63. De Leeuw, G.; Andreas, E.L.; Anguelova, M.D.; Fairall, C.W.; Lewis, E.R.; O'Dowd, C.; Schulz, M.; Schwartz, S.E. Production flux of sea spray aerosol. *Rev. Geophys.* **2011**, *49*, RG2001. [[CrossRef](#)]
64. Batchelor, G.K. *An Introduction to Fluid Dynamics*; Cambridge University Press: Cambridge, UK, 1970; 615p.
65. Ryan, R.T. The behavior of large, low-surface-tension water drops falling at terminal velocity in air. *J. Appl. Meteorol.* **1976**, *15*, 157–165. [[CrossRef](#)]
66. Weiss, R.F. The solubility of nitrogen, oxygen and argon in water and seawater. *Deep-Sea Res.* **1970**, *17*, 721–735. [[CrossRef](#)]
67. Weiss, R.F. Solubility of helium and neon in water and seawater. *J. Chem. Eng. Data* **1971**, *16*, 235–241. [[CrossRef](#)]
68. Weiss, R.F. Carbon dioxide in water and seawater: The solubility of a non-ideal gas. *Mar. Chem.* **1974**, *2*, 203–215. [[CrossRef](#)]
69. Broecker, W.S.; Peng, T.-H. *Tracers in the Sea*; Lamont-Doherty Geological Observatory, Columbia University: Palisades, NY, USA, 1982; 690p.
70. Wanninkhof, R. Relationship between wind speed and gas exchange over the ocean. *J. Geophys. Res.* **1992**, *97*, 7373–7382. [[CrossRef](#)]
71. Millero, F.J. *The Physical Chemistry of Natural Waters*; Wiley-Interscience: New York, NY, USA, 2001; 654p.



© 2017 by the authors. Licensee MDPI, Basel, Switzerland. This article is an open access article distributed under the terms and conditions of the Creative Commons Attribution (CC BY) license (<http://creativecommons.org/licenses/by/4.0/>).